Independent Testing of JWST Detector Prototypes

Donald F. Figer[a], Bernard J. Rauscher[b], Michael W. Regan[a], Ernie Morse[a],
Jesus Balleza[a], Louis Bergeron[a], H. S. Stockman[a]
[a]Space Telescope Science Institute, 3700 San Martin Dr., Baltimore, MD 21218
[b]GSFC, Mail Code 685, Greenbelt, MD 20771

ABSTRACT

The Independent Detector Testing Laboratory (IDTL) is jointly operated by the Space Telescope Science Institute (STScI) and the Johns Hopkins University (JHU), and is assisting the James Webb Space Telescope (JWST) mission in choosing and operating the best near-infrared detectors. The JWST is the centerpiece of the NASA Office of Space Science theme, the Astronomical Search for Origins, and the highest priority astronomy project for the next decade, according to the National Academy of Science. JWST will need to have the sensitivity to see the first light in the Universe to determine how galaxies formed in the web of dark matter that existed when the Universe was in its infancy (z~10-20). To achieve this goal, the JWST Project must pursue an aggressive technology program and advance infrared detectors to performance levels beyond what is now possible. As part of this program, NASA has selected the IDTL to verify comparative performance between prototype JWST detectors developed by Rockwell Scientific (HgCdTe) and Raytheon (InSb). The IDTL is charged with obtaining an independent assessment of the ability of these two competing technologies to achieve the demanding specifications of the JWST program within the 0.6-5 μm bandpass and in an ultra-low background (<0.01 e^-/s/pixel) environment. We describe results from the JWST Detector Characterization Project that is being performed in the IDTL. In this project, we are measuring first-order detector parameters, i.e. dark current, read noise, QE, intra-pixel sensitivity, linearity, as functions of temperature, well size, and operational mode.

Keywords: near-infrared detectors, characterization, JWST, NGST, NIR

1. INTRODUCTION

The James Webb Space Telescope (JWST) is regarded as the most important space astronomy mission for the next decade. As the centerpiece of the NASA Office of Space Science (OSS) theme: *the Astronomical Search for Origins,* the JWST will study the origins and evolution of galaxies with the sensitivity to see the first light in the Universe (z ~10-20). The JWST will be a 6.5-m class telescope located near L2 and optimized for the 1-5 μm waveband. Its goal is to detect sources as faint as magnitude 33 (<one photon per second at the detector) to fully exploit its potential.

Sensitive detectors are important for JWST, given the desire to observe the redshifted light from the early Universe. The natural background due to sunlight scattered by and thermal emission from interplanetary (zodiacal) dust in the Solar System is low in the 1–4 μm range, a range in which the apparent spectral energy distributions of high-z (z~1–10) galaxies are maximum. Both imaging and spectroscopic observations are required in the NIR, and NIR detectors will be the primary sensors for guiding and establishing/maintaining the wave front performance of the telescope. There are two basic challenges associated with developing these detectors. To achieve JWST's planned sensitivity limit, the detectors must be more sensitive than those flown on previous missions. The detector will be the dominant noise source for spectroscopy of faint sources, assuming read noise of 3 e^- and dark current 0.02 e^-/s. Note that the NICMOS HgCdTe detectors on the Hubble Space Telescope have minimum read noise of 18 e^- (25 samples, up-the-ramp) and dark current ~0.05 e^-/s, while SIRTF InSb detectors are expected to exhibit a minimum read noise of 10 e^- (64 samples, Fowler sampling) and dark current <1 e^-/s.

The JWST Project has funded both Raytheon Vision Systems and Rockwell Scientific to produce near-infrared array detectors for evaluation against the challenging requirements of the NIRCam, NIRSpec, and FGS. These instruments require 10, 2, and 4 2048X2048 array detectors, respectively. Craig McCreight (NASA/Ames Research Center) led the NASA development program that provided the vendors the resources to build a series of progressively more capable devices, and culminated in the deliveries of $2K^2$ "home run" devices for comparative testing. Given the original goal of developing working technology by September 2003, this program has been a great success.

In parallel with the detector development program, NASA funded a detector-testing program, which was also led by Craig McCreight. Three laboratories, selected through a competitive proposal process, evaluated the products of the development program in conditions similar to that expected for JWST, i.e. ultra-low backgrounds. The test groups were announced in January 2001 and include University of Hawaii (PI Don Hall), University of Rochester (PI William Forrest), and STScI/JHU (PI Don Figer). NASA Ames (R. McMurray, M. McKelvey, & C. McCreight) was also a member of the JWST test network, with primary responsibilities for testing the mid-infrared technology and performing radiation testing of the near-infrared devices.

STScI/JHU established the Independent Detector Testing Laboratory (IDTL) to provide the detector testing data that informs the best decision for choosing which detectors will be used on JWST. Rockwell and Raytheon have provided a series of JWST prototype detectors to the IDTL for comparative testing. Using a set of standardized procedures, the IDTL has characterized these detectors, collecting and analyzing over 2 Terabytes of data that are now offered on the IDTL Web/FTP site.

In this paper, we describe the test program and results that were obtained in the JWST Detector Characterization (JDC) project in the IDTL. After a challenging and highly successful detector development and testing programs, the James Webb Space Telescope (JWST) is poised to benefit from the best infrared array detectors ever made. The University of Arizona chose HgCdTe detectors made by Rockwell Scientific Company for use in the Near-Infrared Camera (NIRCam). NASA/JPL chose Si:As detectors made by Raytheon Vision Systems (Fig. 2) for use in the Mid-Infrared Instrument (MIRI). Three $1K^2$ Si:As detectors will be needed in the current MIRI design. The Near-Infrared Spectrograph (NIRSpec) and the Fine Guidance Sensors (FGS) teams are expected to announce their final selections soon.

2. PROJECT GOALS

Quoting from the original project proposal, we proposed to *"...measure first-order detector properties (read noise, dark current, persistence, quantum efficiency, etc.) as functions of environmental parameters (radiation exposure, thermal conditions, operating modes) for both detector types, using the same procedures, setups, dewars, light sources, targets, electronics, acquisition software, analysis software, and staff."* The novel value of this approach rests in the fact that the data measured for both technologies are directly comparable. While systematic errors are always a concern in detector characterization, the approach in this project ensures that any such errors are similar in characterizations of all detectors that are tested.

3. IDTL SYSTEM

In order to realize the project goals, we built a system that could reliably obtain large volumes of data and reduce/analyze those data in near-real time. The IDTL system was described extensively in Figer et al. (2003). Briefly, the system includes an ultra-low background facility that can accommodate a 6KX6K cryogenic focal plane. The detectors can be tested with minimal modification for different detector array types. Blackbody and monochromator sources were placed outside the dewar. There are two cold mechanisms in the dewar in front of the detector that contain a filters and cold blanks for the dark current and latent charge tests. A single detector enclosure is used to provide a light-tight cavity around the detector. The electronics system was the same for both types of detectors, although individual fanout boards were custom fabricated.

4. ELECTRONIC GAIN/CONVERSION GAIN

The IDTL experiment suite includes procedures to determine both the internal (MUX) electronic gain and the conversion gain (electrons per ADU) for detectors from both vendors. The internal electronic gain is defined as the gain from the unit cell to the output of the Read Out Integrated Circuit (ROIC or "MUX"). Conversion gain relates output values in ADU to the corresponding number of electrons at the unit cell. Table 1 displays the results for these two experiments for the Raytheon SB304-008-5.0mu and Rockwell H2RG-015-5.0mu devices. The conversion gain values of 1.3 e^-/ADU and 2.2 e^-/ADU for the Rockwell and Raytheon devices, respectively, should be used to interpret results in ADU throughout the remainder of this document.

The electronic gain experiment begins by shielding the detector from external light sources by commanding both filter wheels to put the unmachined blank in place. Then the detector's reset voltage is sequentially set to several different values and a CDS (correlated double sampling) image with the minimum possible exposure time is taken at each setting. Once this process is complete, the median signal in the first read of each of the CDS exposures is plotted vs. the corresponding value of the reset voltage. A linear least-squares fit is then performed on the data and the slope of the resulting line is taken as the electronic gain expressed in microvolts per ADU. Signal vs. reset voltage plots for the Raytheon and Rockwell devices are presented as Figure 2 and Figure 1.

The conversion gain experiment was performed using the photon transfer or variance method, which involves plotting variance vs. signal in ADU, performing a linear least-squares fit and quoting the conversion gain as the inverse of the slope of the resulting line. We performed two different variations of this experiment, with good agreement existing between the results obtained by the two methods.

The first variation of the experiment (full-frame method) depends on uniform illumination of the entire array. Results are obtained for J, H, K, L and M band-pass filters at the optimum detector temperature for the device being tested. A constant light source is employed, and a group of 10 CDS exposures is taken at each of a sequence of 8 logarithmically spaced exposure times. After the data acquisition is complete, each of the 10 CDS exposures in a group are processed by subtracting the first read from the second read. A similarly-processed dark frame of matching exposure time is then subtracted from each processed frame. The 10 processed frames are then combined in a data cube and the median value and standard deviation of the 10 values for each detector pixel is calculated. This process is repeated for the groups of exposures taken at each of the exposure times. For each exposure time group, a signal value is obtained by taking the median of all of the individual pixel median values. A variance value for the group is obtained by taking the median of all of the individual pixel standard deviations. Once a signal-variance data point is obtained for each exposure time, the data points can be displayed in a plot of variance vs. signal. A least-squares fit is performed and the inverse of the slope of the fitted line is reported as the conversion gain in electrons per ADU. See Figure 3 for a typical plot produced using this method.

The second variation of the experiment (gray scale method) requires variable illumination across the array. A gray scale target (see Figure 5) placed between a constant light source and the dewar window achieves this effect on the focal plane array. For each band pass filter, 10 CDS exposures are taken at a specified exposure time. The CDS frames are processed and dark subtracted as in the first variation and the median and variance are calculated for each pixel. These values are grouped into signal histogram bins and a median signal and variance are calculated for each bin. The resulting signal-variance data points are then plotted and the conversion gain is determined as in the full-frame method. See Figure 4 for a typical plot produced using this method.

Part	ext. gain	int. gain	MUX gain	conv. gain	conv. gain	C_{cell}
	μV/ADU	μV/ADU	gain	e^-/ADU	e^-/μV	fF
H2RG-015-5.0mu	3.81	4.31	0.89	1.30	0.30	48

Part	ext. gain	int. gain	MUX gain	conv. gain	conv. gain	C_{cell}
	μV/ADU	μV/ADU	gain	e^-/ADU	e^-/μV	fF
SB304-008-5.0mu	3.81	4.83	0.79	2.20	0.46	73

Table 1. Summary of gain and capacitance values for Rockwell (top) and Raytheon (bottom) devices. The conversion gain has been used to convert all IDTL results originally produced in ADU to electrons for these two devices.

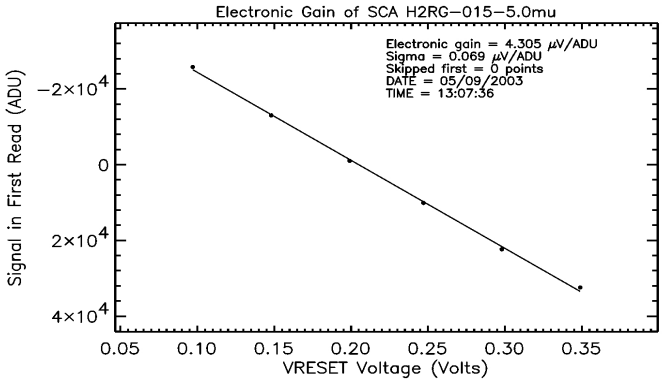

Figure 1: Electronic gain plot for Rockwell H2RG-015-5.0mu device.

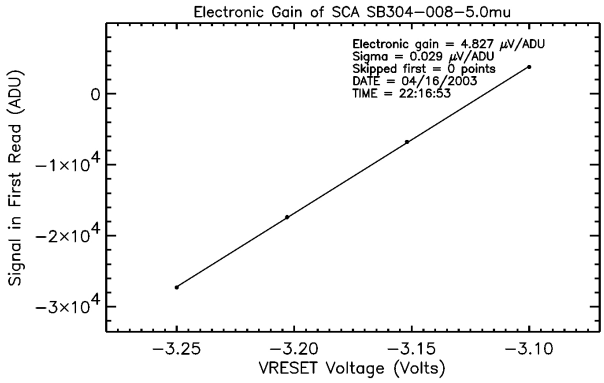

Figure 2: Electronic gain plot for Raytheon SB304-008-5.0mu device.

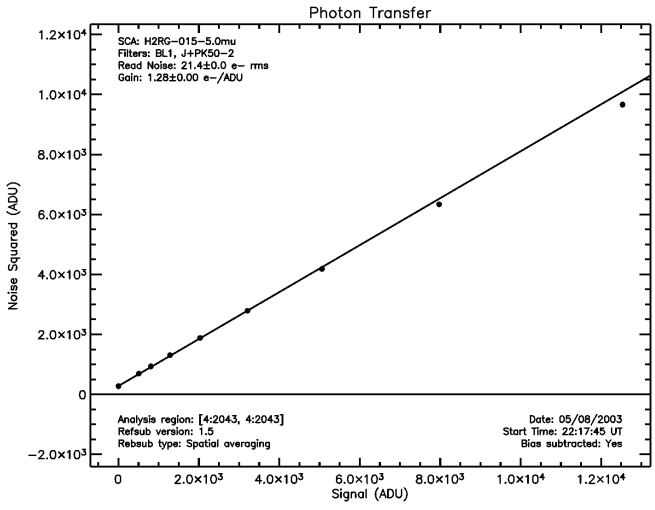

Figure 3: Output from full-frame conversion gain experiment.

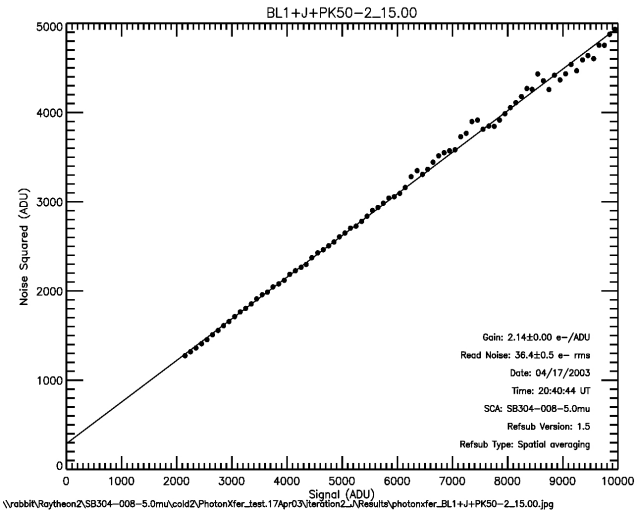

Figure 4: Output from gray scale conversion gain experiment.

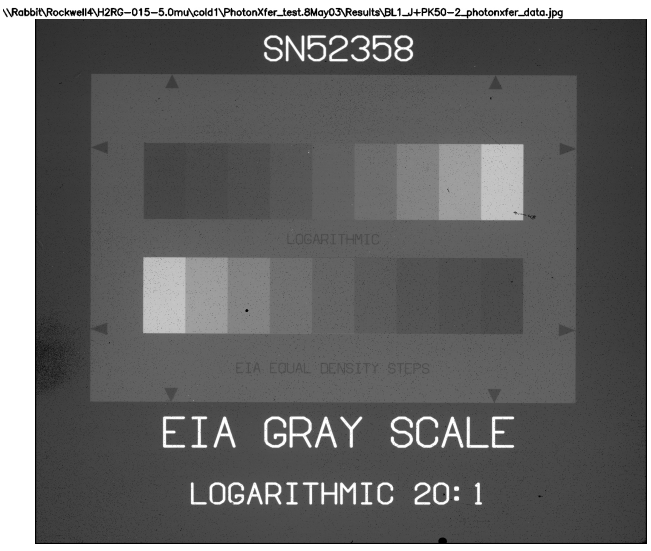

Figure 5: Image of gray scale target used in variation of conversion gain experiment.

The linearity experiment seeks to characterize the departure of a measured count rate from its expected value as a function of the number of electrons (fluence) in the detector well. Data collected for the full-frame variation of the conversion gain experiment are used for this purpose. Linearity behavior of a detector can be quantified by solving for the coefficients in the equation

$$countRate = 1 - aDN - bDN^2 .$$

Figure 7 shows the calculated values for the equation coefficients for both the Rockwell and Raytheon devices.

Device	Linear term(e^-)	Quadratic Term (e^-)
SB304-008	4.4×10^{-6}	9.4×10^{-11}

Device	Linear term(e^-)	Quadratic Term (e^-)
H2RG-015	9.3×10^{-7}	9.0×10^{-12}

Table 2. Non-linearity coefficients for Rockwell H2RG-015-5.0mu (bottom) and Raytheon SB304-008-5.0mu (top).

Another way to characterize detector non-linearity is to quote the detector fluence where the deviation from the expected countrate reaches 10%. This threshold is reached at a fluence of 77000 electrons for the Raytheon SB304-008-5.0mu device and at a fluence of 104000 electrons for the Rockwell H2RG-015-5.0mu device. See Figure 6.

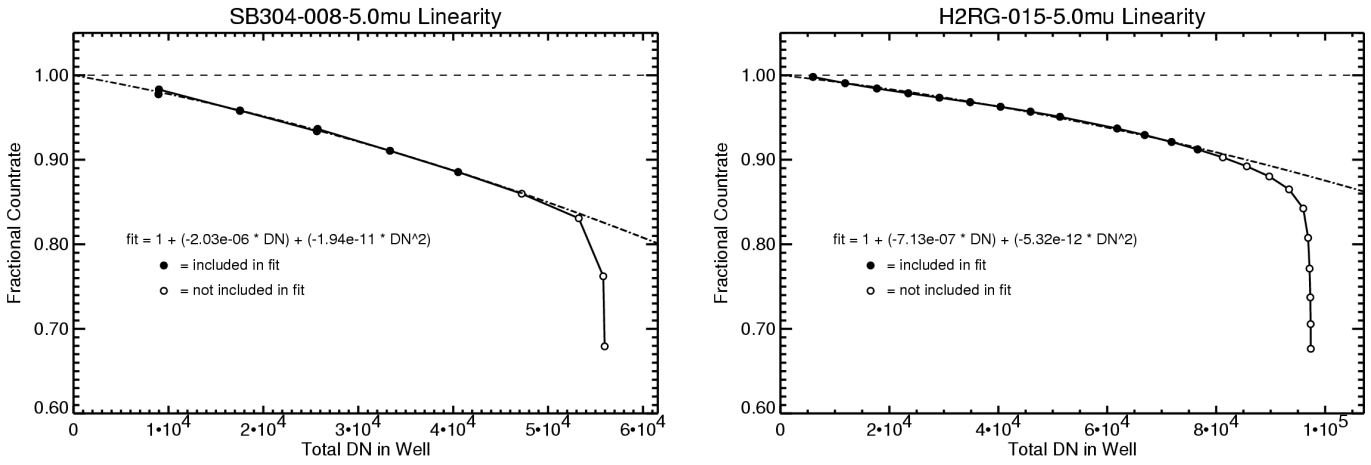

Figure 6: Inferred count rate as a function of measured signal for the Raytheon SB304-008-5.0mu device (left) and the Rockwell H2RG-015-5.0mu device (right). The experiment is performed at optimum operating temperature for each device. Results are shown in ADU and thus must be multiplied by the appropriate conversion gain to determine values in electrons. The K+PK50-2+BL2 filter combination refers to a K band-pass filter, a 2mm PK50 filter and a sandwich of two 1% Inconel neutral density filters.

5. LINEARITY/WELL DEPTH

Well capacity is a measure of the amount of signal (in electrons) that detector pixels can record before saturating. The NIRCam requirement for well capacity is 60000 electrons, with a goal of 200000 electrons.

The gain of the IDTL testing system is too large to allow sampling of the entire well capacity before the maximum output value of the analog-to-digital converter is reached. In order to surmount this difficulty, the IDTL well capacity test requires the taking of two exposures, one to sample the zero-level of the well, and one to sample near the saturation level.

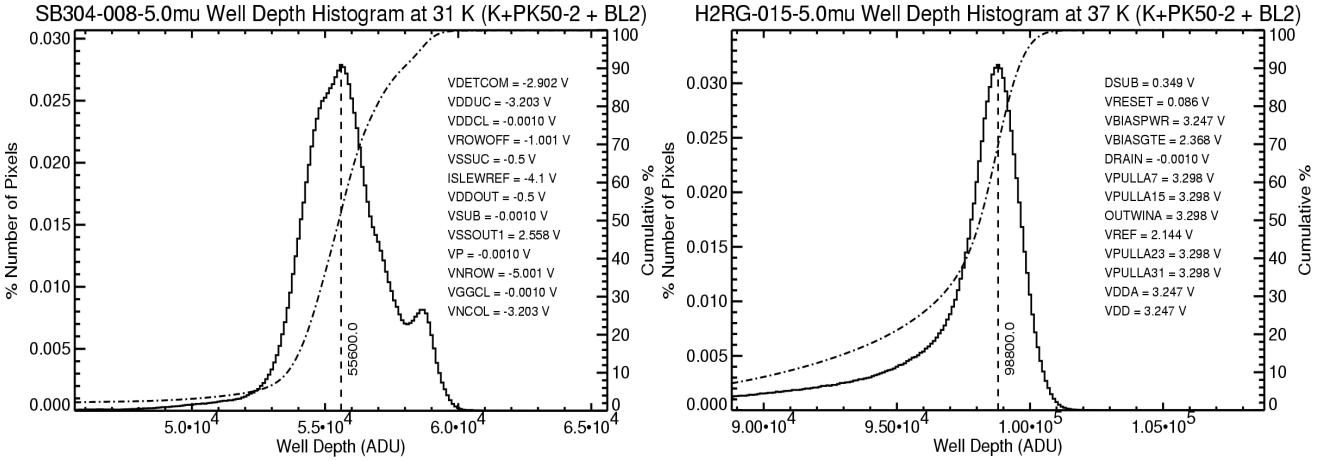

Figure 7: Well capacity histograms for the Raytheon SB304-008-5.0mu device (left) and the Rockwell H2RG-015-5.0mu device (right). Experiment is performed at optimum operating temperature for each device. Results are shown in ADU and thus must be multiplied by the appropriate conversion gain to determine values in electrons. The K+PK50-2+BL2 filter combination refers to a K band-pass filter, a 2mm PK50 filter and a sandwich of two 1% Inconel neutral density filters.

The experiment begins by setting up a suitable light source, setting the detector temperature to the optimal operating temperature for the device being tested and putting the desired filters in place. After setup is complete, the experiment proceeds with the taking of a sampled-up-the-ramp (SUTR) image with an exposure time selected so that the measured signal reaches the top end of the A-D range before the end of the exposure. The system video offset is then changed to a value such that a subsequent SUTR exposure reaches saturation before the top end of the A-D range. The second SUTR exposure is then taken.

Once two suitable SUTR exposures have been acquired, the signal offset (in ADU) between the two exposures is calculated. The first read of the zero-level exposure is then subtracted from the last read of the full-well exposure and the offset is added to the difference. A histogram of signal is created from the population of saturated pixels and the histogram peak is reported as the well capacity.

The IDTL experiment measures a well capacity of 122000 electrons for the Raytheon SB304-008-5.0mu device and a well capacity of 130000 electrons for the Rockwell H2RG-015-5.0mu device (see Figure 7).

6. DARK CURRENT

The dark current is taken to be the portion of electronic charge that accumulates in a detector in the absence of exposure to light. The JWST NIRCam Requirement is <0.01 e^-/sec/pixel, and the IDTL measurement goal is <0.001 e^-/sec/pixel.

For the dark current experiment, we obtained image cubes containing data from a number (8 or 250) of non-destructive samples up-the-ramp (SUTR). The array was read out continuously for the 250 read cube so that it took 2700 seconds to complete all reads. The 8 read cube was obtained through equally spaced reads over a time span of 1340 seconds. We generally obtained the SUTR-8 cubes during the "settling" phase of the experiment covering the first 10 to 20 hours. During this phase, the temperature was set to the "nominal" value given to us by the vendors (37 K for Rockwell and 30 K for Raytheon). At the end of the settling period, we obtained the three to six SUTR-250 cubes, first at the nominal temperature and then over a range including, T=26 K, 28 K, 30 K, 32 K, 35 K, 37 K, 40 K, 45 K, 50 K, 60 K, 70 K, 80 K.

The results are given in Table 3 and Table 4. The table entries are in units of electrons per 1000 seconds per pixel and represent the median slope of fits to individual pixels in a 250 read cube over 2700 seconds. We used the SUTR-250 and SUTR-8 cubes to infer a contribution to the accumulating charge as a function of the number of reads, finding ~0.01-0.03 e^-/read for the Rockwell part and ~0.17 e^-/read for the Raytheon part. The results show excellent performance, with dark currents <0.01 e^-/sec/pixel for the Rockwell device at temperatures of 50 K and below, and for the Raytheon device at 28 K (after subtracting effects of the "per-read" contribution).

Note that the SUTR-8 measurements with the Rockwell device gives a current density of 400 e^-/sec/cm^2, the lowest ever measured for a 5 μm device, according to Figure 2 of Finger & Beletic (2003).

The following figures show a sampling of the IDTL dark current measurements. The figure titles and legends contain information concerning the detector type, region of analysis, and software version of the reference pixel correction. In general, we used the spatial averaging technique for reference pixel correction, as described by Rauscher et al. (2003).

Table 3. Dark current results for H2RG-015-5.0 µm. The values in the table are in e⁻/1000 sec/pixel and represent the slope of the best line fit for SUTR-250 image cubes.

Part	Temperature (K)											
	26	28	30	32	35	37	40	45	50	60	70	80
H2RG-015-5.0mu	NA	4.0	4.6	3.9	4.0	3.9 *	5.6	9.1	13	30	103	1004

*1.5-2.4 e^- measured using UTR-8. We infer a "per read" contribution of ~0.01-0.03 e^-/read.

Table 4. Dark current results for SB304-008-5.0 µm.

Part	Temperature (K)											
	26	28	30	32	35	37	40	45	50	60	70	80
SB304-008-5.0mu	NA	22 *	35	64	205	689	4659	61415	NA	NA	NA	NA

*6 e^- measured using UTR-8. We infer a "per read" contribution of ~0.17 e^-/read.

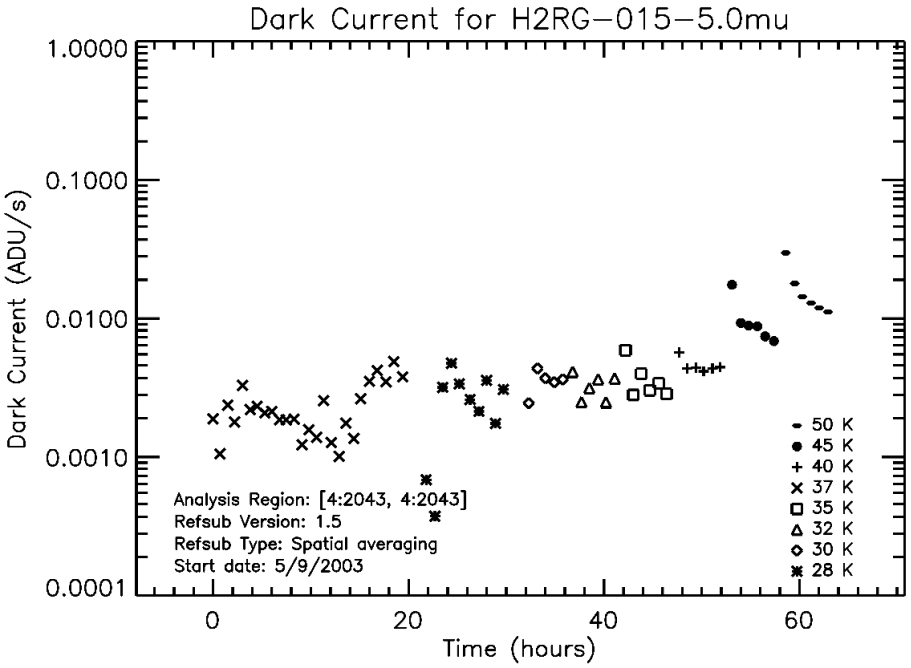

Figure 8. Dark current measurements versus temperature. The values represent the median slope of fits to accumulating charge in 250 reads of each pixel over 2700 seconds. The first 17 hours of data were taken in the SUTR-8 read mode.

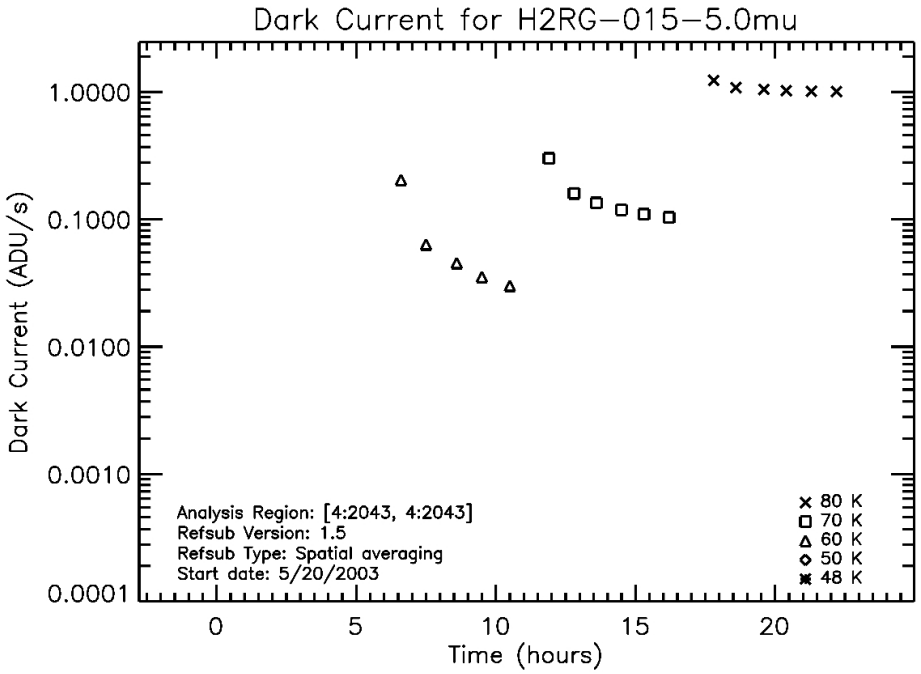

Figure 9. Dark current measurements versus temperature. The values represent the median slope of fits to accumulating charge in 250 reads of each pixel over 2700 seconds.

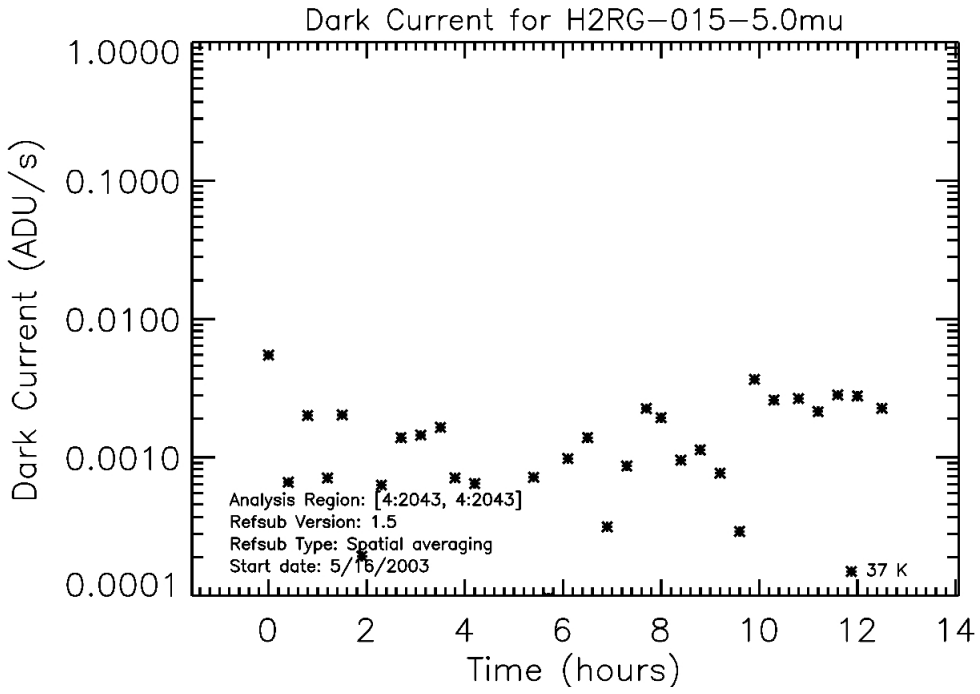

Figure 10. Dark current measurements versus temperature. The values represent the median slope of fits to accumulating charge in 8 reads of each pixel over 1340 seconds.

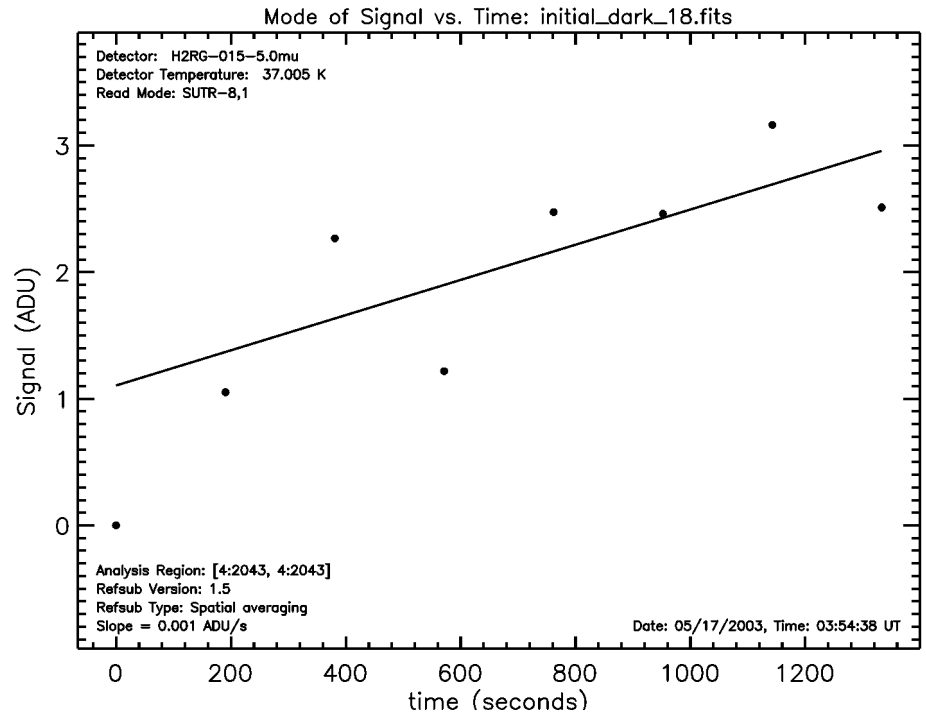

Figure 11 Signal versus time for SUTR-8 image cube.

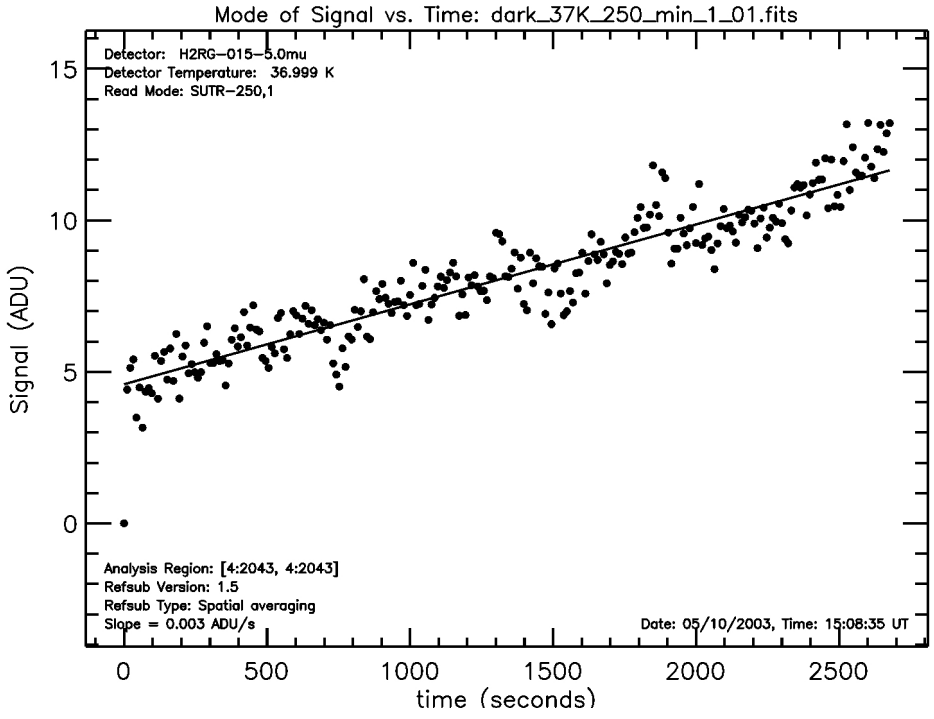

Figure 12. Signal versus time for SUTR-250 image cube.

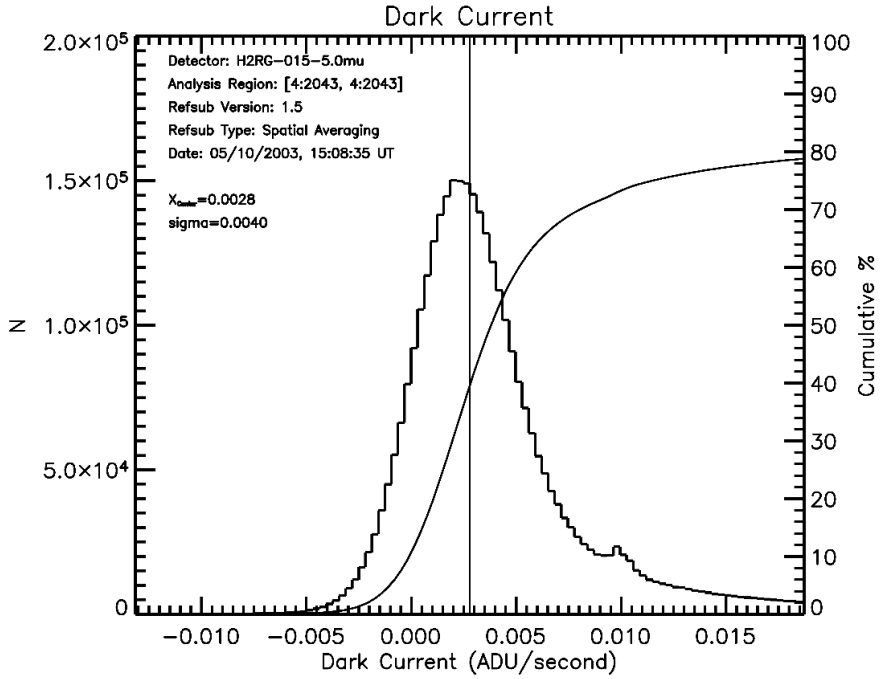

Figure 13. Histogram of dark current values for all pixels in SUTR-250 frame for T=37 K. The median and cumulative counts are overplotted.

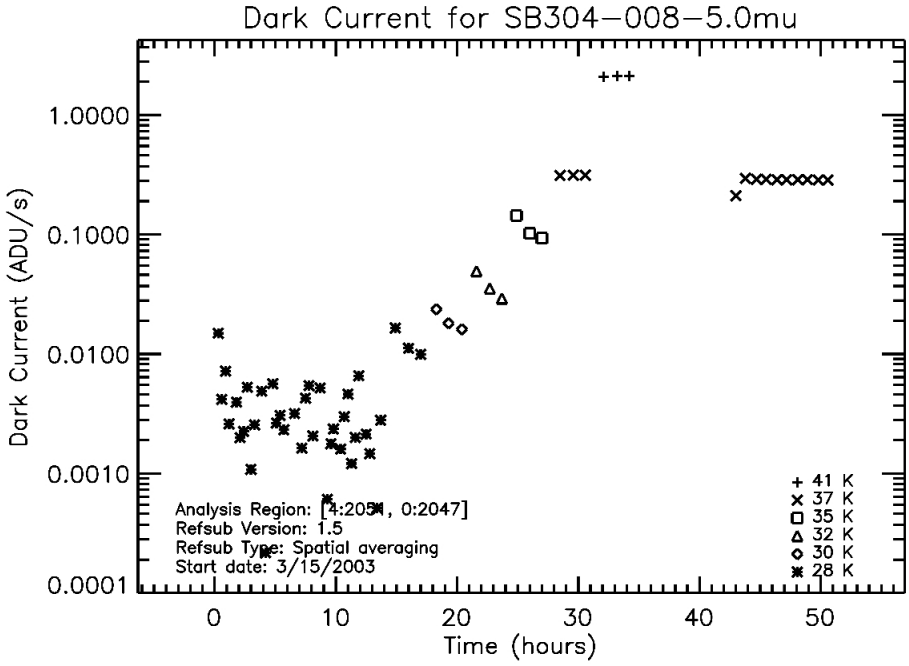

Figure 14. Dark current measurements versus temperature. The values represent the median slope of fits to accumulating charge in 250 reads of each pixel over 2700 seconds. The first 10 hours of data were taken in the SUTR-8 read mode.

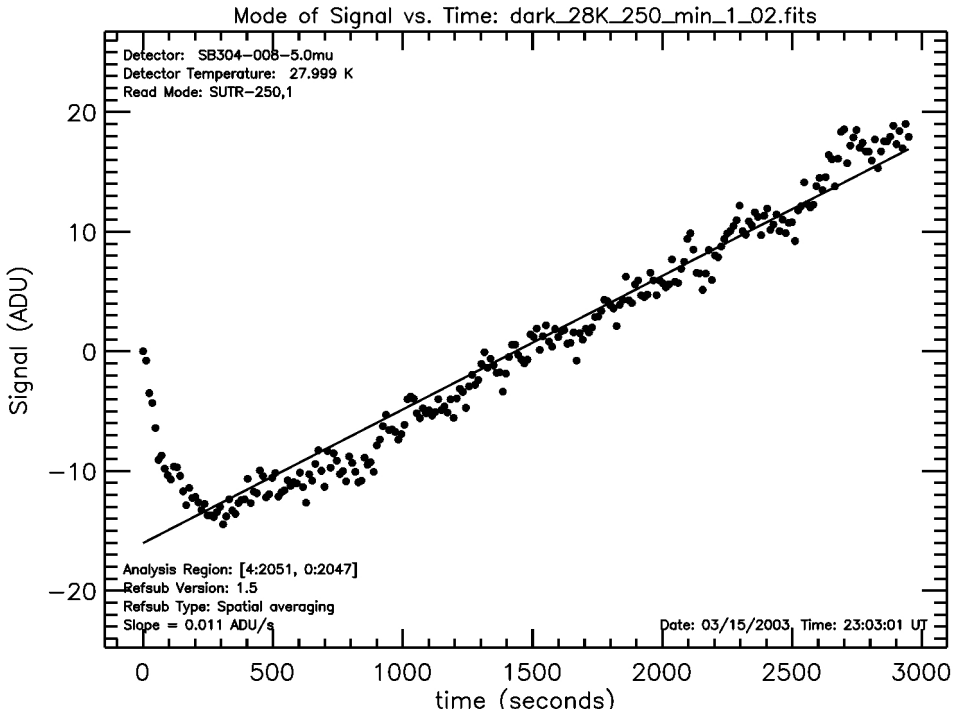

Figure 15. Signal versus time for SUTR-250 image cube.

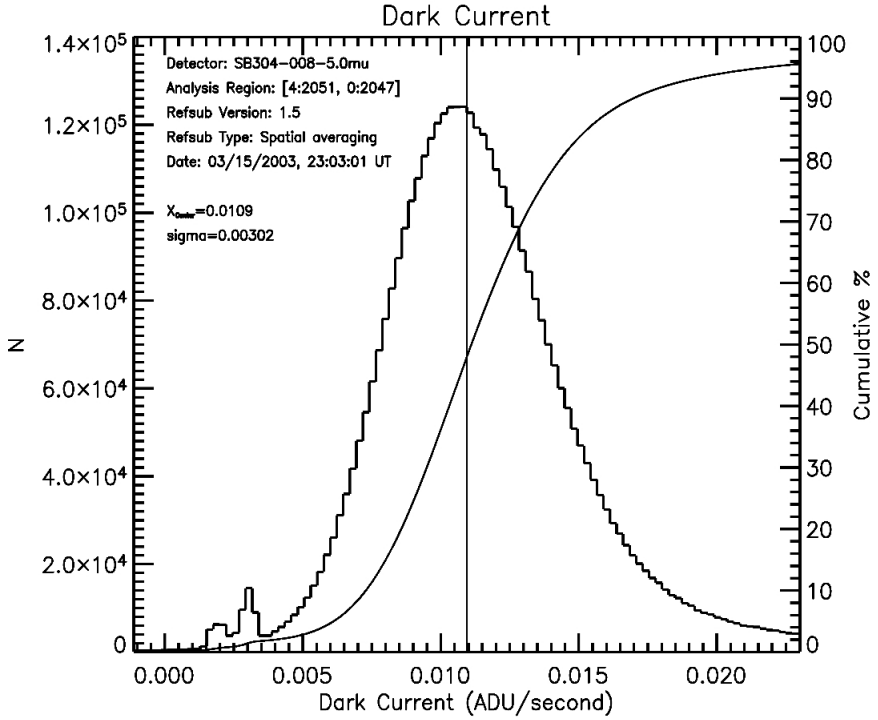

Figure 16. Histogram of dark current values for all pixels in SUTR-250 frame for T=37 K. The median and cumulative counts are overplotted.

7. READ NOISE

Read noise is the uncertainty in estimating the charge in a pixel. To allow the detector vendors leeway in optimizing their designs, the JWST project specifies both the total noise (including read noise and shot noise on integrated dark current) in t=1000 s Fowler-8 sampled exposures and the read noise for a single read. The read noise for a single read is the uncertainty in estimating the charge for a single analog-to-digital converter conversion. The NIRCam noise requirements are: (1) total noise per 1000 seconds Fowler-8 exposure ≤9 e^- rms and (2) read noise for a single read ≤15 e^- rms. The corresponding NIRSpec requirement is total noise per 1000 seconds SUTR-84 sampled exposure ≤6 e^- rms. In a SUTR-84 sampled exposure, the SCA is sampled 84x continuously going up the ramp.

An essential part of measuring read noise is understanding the noise properties of the detector readout system. The IDTL readout system was characterized by mounting 2 K shorting resistors where the SCA would normally mount to the cryogenic harness. Shorting resistor tests were made using the full cable harness, routed through the dewar in the cryogenic configuration, with a shorting resistor block replacing the SCA. Figure 17 shows the schematic diagram for shorting resistor tests that was agreed among the four JWST ultra-low background test facilities.

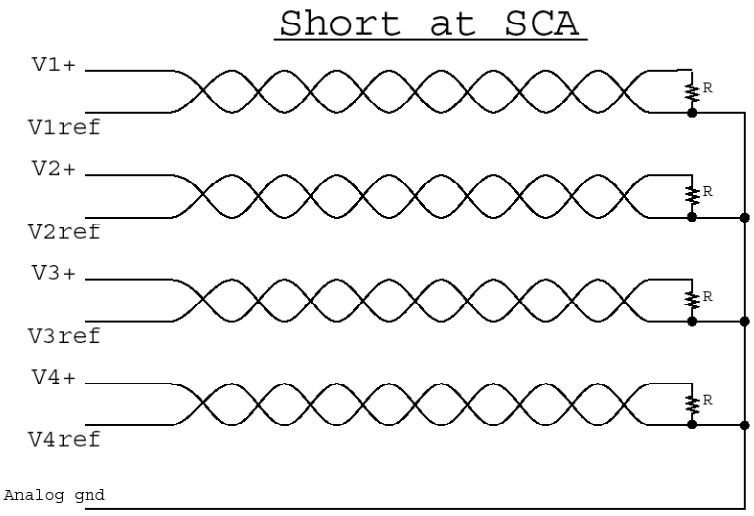

Figure 17. In order to measure IDTL system noise, 2 K shorting resistors were mounted where the SCA normally connects to the cryogenic harness.

In the case of the Rockwell HAWAII-2RG test setup, the IDTL system showed little excess high-frequency noise (compared to the measured total noise) in either the temporal or spatial domains (see Figure 18). The IDTL setup does have somewhat more low frequency (~1/f) noise than e.g. the University of Hawaii setup, which uses a slightly modified version of the Leach controller used in the IDTL. Some of Hawaii's modifications were specifically aimed at reducing 1/f noise. We believe that this probably explains the difference in the low frequency noise properties of the two test setups. For the Rockwell HAWAII-2RG SCA, our measurements indicate that the IDTL system contributes about 8 e- of noise per correlated double. This corresponds to about 3 e^- rms per Fowler-8 exposure which is adequate for JWST detector testing.

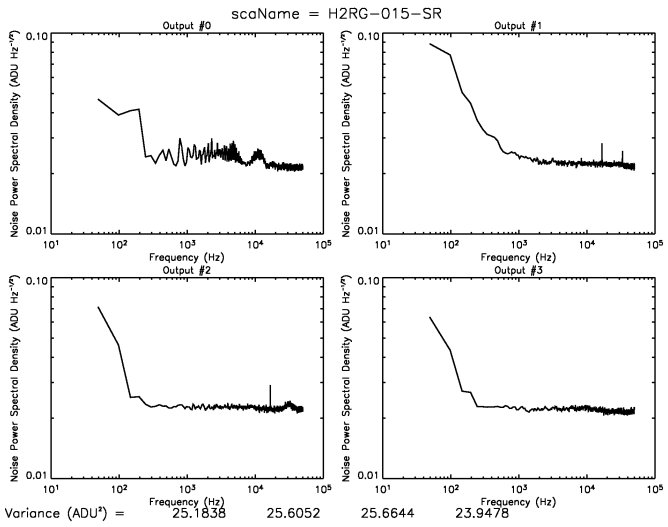

Figure 18. The Fourier Power Spectrum of the IDTL test setup for Rochwell HAWAII-2RG SCAs is mostly flat. The most obvious component is a ~1/f tail at low frequencies. Our measurements indicate that the test setup contributes about 8 e- rms per correlated double sample in this configuration. This corresponds to about 3 e^- rms per Fowler-8 exposure which is well below the JWST 9 e^- requirement for the detector.

The IDTL test setup unfortunately showed excess high frequency noise for testing the Raytheon SB-304 SCA. We believe that this noise was caused by a known ground loop running from the Leach controller ground, through the dewar, and back to the building ground via the cryocooler's helium lines. We have subsequently broken this ground loop, and preliminary indications are that the system noise is now lower than it was during the testing reported here. The shorting resistor configuration was the same as for testing the HAWAII-2RG setup. Figure 19 shows the resulting noise power spectra.

As can be seen in Figure 19, the Fourier Power Spectrum shows noise spikes at frequencies greater than about 1 kHz. The flat portion of the spectrum is also elevated compared to the HAWAII-2RG test setup. This behavior is caused by spikes in the temporal domain. The effect of these temporal spikes can be seen as an alternating 4-columns pattern in the difference between two dark images (See Figure 19). The alternating 4-column pattern arises because the Raytheon SB-304 SCA has 4 interleaved outputs. As such, groups of 4 pixels are readout out simultaneously. The noise of the test setup in the SB-304 configuration is about 18.9 e^- per correlated double sample. Because the noise is correlated, it is not possible to straightforwardly scale this to Fowler-8 sampling. Using digital filtering, the IDTL system contributes about 8.8 e^- per correlated double sample of noise.

To allow testing of the SB-304 SCA, we developed a simple digital filter to remove the pattern noise. Within each group of 4 pixels, the average of 3 pixels was subtracted from the pixel of interest. As can be seen in the right-hand pane of Figure 20, the filter is effective at removing the pattern noise. It unfortunately also removes some 1/f. As such, the use of the digital filter probably causes us to underestimate the noise of the Raytheon SB-304 SCA somewhat compared to the Rockwell HAWAII-2RG.

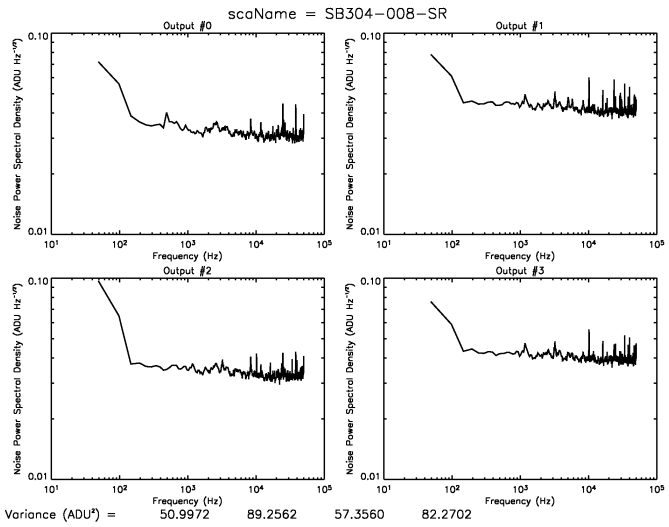

Figure 19. The IDTL test setup for the Raytheon SB-304 SCA showed excess high frequency noise, notice the many spikes at high frequency. The flat portion of the spectrum is also higher than for the HAWAII-2RG setup. This behavior can be caused by spikes in the temporal domain, the effect of which can be seen in Figure 20.

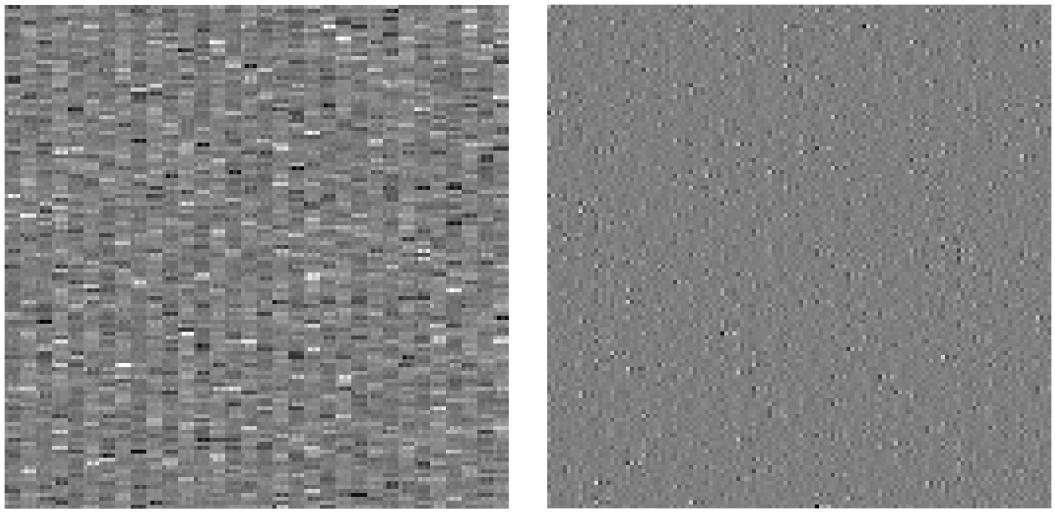

Figure 20. The IDTL test setup showed excess pattern noise for testing the SB-304 SCA. Shown at left is the image of a 2 K shorting resistor mounted where the SCA normally connects. The alternating 4-columns pattern arises from temporal spikes at frequencies faster than the ~100 kHz pixel rate. In the SB-304, the 4 outputs are interleaved. Hence, the first group of 4 columns is read out simultaneously, and likewise for the remaining groups of 4 columns. Shown at left is the result of digitally filtering out the alternating 4-columns pattern. Within each group of 4 pixels, the average of the 3 remaining pixels was subtracted from the pixel of interest. The noise in the unfiltered image at left is about 18.9 e^- per correlated double sample. Noise in the filtered image at right is about 8.8 e^- per correlated double sample.

Data for the read noise experiment are extracted from the same files taken for the dark current experiment (see Section 6). In plots of read noise versus the number of Fowler frames (Fowler-n), the exposure time is always the shortest that is required to obtained the required number of samples. For example, with a 10 second frame time, a Fowler-8 exposure has an =80 seconds exposure time. For measuring Total Noise, the exposure time was fixed at =1000 seconds. As is the case in the dark current experiment, data are obtained at a range of temperatures.

The results are given in Table 5 and Table 6. To within the uncertainties of the measurements, we believe that the Rockwell HAWAII-2RG and Raytheon SB-304 have roughly comparable read noise per read. Although we do not report Total Noise for the Raytheon SB-304 on account of the difficulty of filtering out the pattern noise in Fowler-n sampled images, we believe that the SB-304 would show higher total noise on account of the higher dark current (see Section 6). This would be especially true if the detectors had to be operated at temperatures T>30 K for either planned or unplanned reasons.

The following figures show a sampling of the IDTL read noise and total noise measurements. The figure titles and legends contain information concerning the detector type, region of analysis, and software version of the reference pixel correction. In general, we used the spatial averaging technique for reference pixel correction, as described by Rauscher et al. (2003).

Table 5. Total Noise and Read Noise of Rockwell HAWAII-2RG

Part	*Experiment*	***Temperature (K)***							
		28	***30***	***32***	***35***	***37***	***40***	***45***	***50***
H2RG-015-5.0mu	***Total Noise***[1]	11.7	11.0	11.0	10.3	10.3	10.3	10.3	11.2
	Read Noise per Read	16.8	16.3	16.3	15.6	15.6[2]	15.4	14.8	14.8

[1]Total noise per t=1000 seconds Fowler-8 exposure
[2]=12.5 in horizontal reference pixels which tends to filter out 1/f noise.

Table 6. Total Noise and Read Noise of Raytheon SB-304

Part	Experiment	***Temperature (K)***							
		28	***30***	***32***	***35***	***37***	***40***	***45***	***50***
SB304-008-5.0mu	***Total Noise***	NA	NA	NA	NA	NA	NA	NA	NA
	Read Noise per Read[2]	NA	10	NA	NA	NA	NA	NA	NA

[2]Estimated using digitally filtered data. The IDTL system showed excessive pattern noise for testing this part.

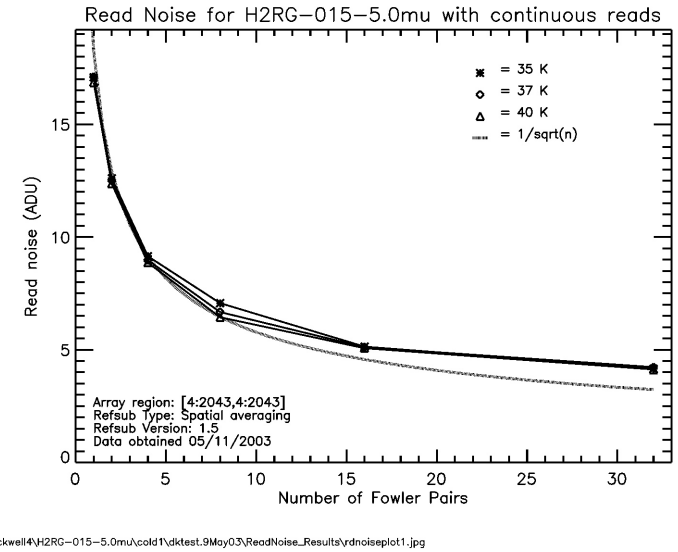

Figure 21. Read Noise for SCA H2RG-015-5.0mu versus Fowler Number.

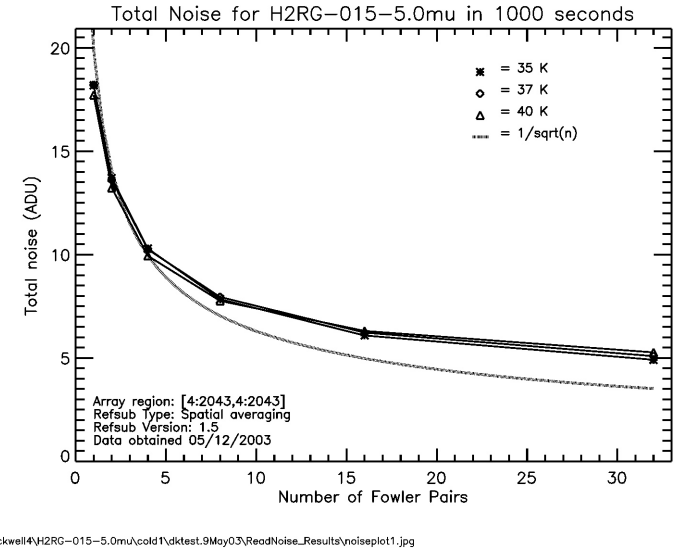

Figure 22. Total Noise for SCA H2RG-015-5.0mu versus Fowler Number.

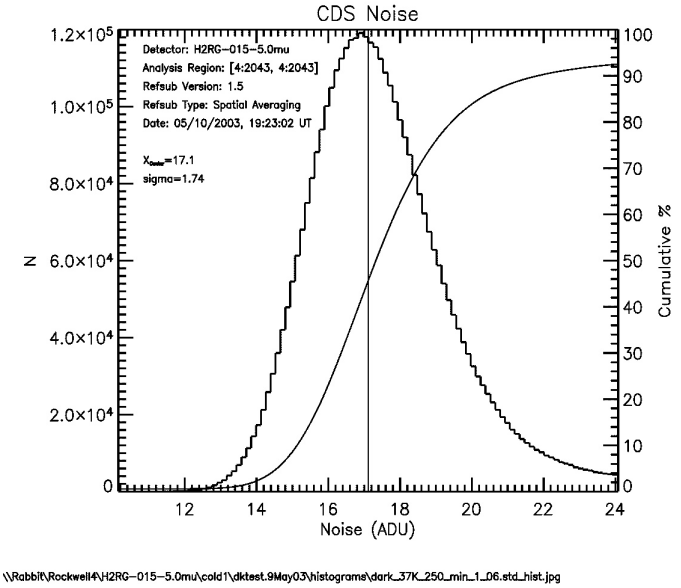

Figure 23. Histogram of Correlated Double Sampling Read Noise in SCA H2RG-015-5.0mu

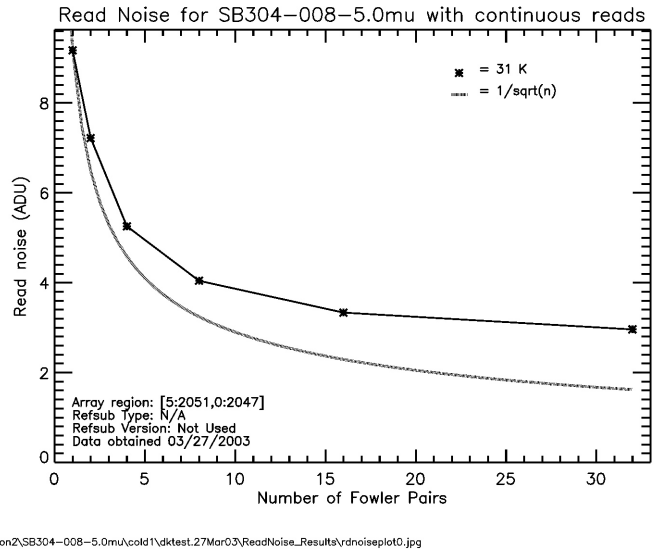

Figure 24. Read Noise for SCA SB304-008-5.0mu versus Fowler Number. This is an upper limit. As discussed in the text, the IDTL test setup showed excess pattern noise for testing this part.

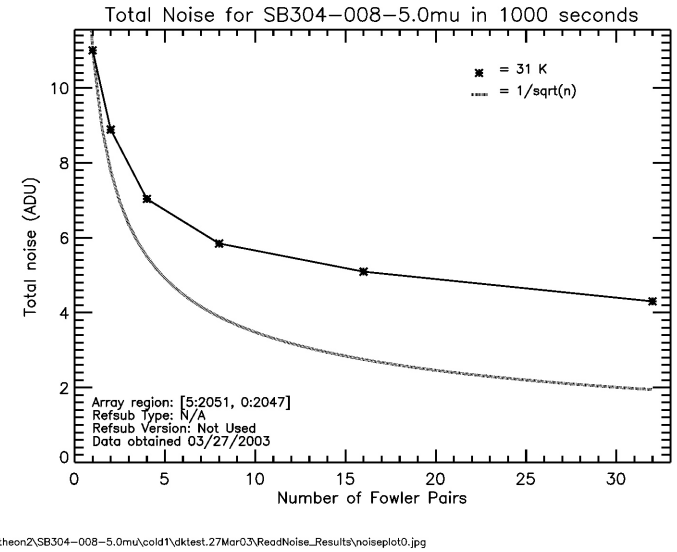

Figure 25. Total Noise for SCA SB304-008-5.0mu versus Fowler Number. This is an upper limit. As discussed in the text, the IDTL test setup showed excess pattern noise for testing this part.

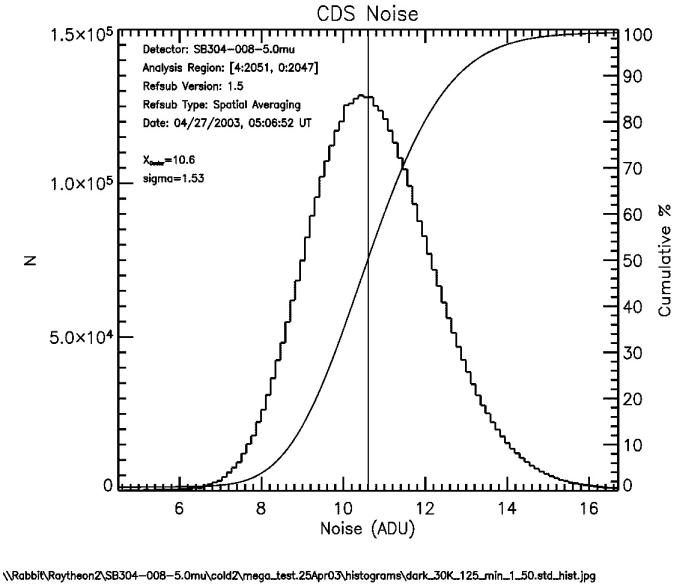

Figure 26. Histogram of Correlated Double Sampling Read Noise in SCA SB304-008-5.0mu. Noise is an upper limit. As discussed in the text, the IDTL test setup showed excess pattern noise for testing this part.

8. PERSISTENCE

Latent charge, or "persistence," is the portion of the signal that is produced by sources in previous images. Anything that liberates charge into the conduction band can result in latent charge, i.e. a bright star or a cosmic ray. Note that latent images are distinguished from spurious sources produced by settling effects in the post-detector analog electronics, i.e. electronic "ghosts" or crosstalk between electronic readout channels. Latent charge is a function of incident flux during a previous exposure, total charge collected during a previous exposure (fluence), the amount of time since the previous exposure, the applied reverse bias on the unit cell, and temperature.

The NIRCAM requirement is <0.1% after the 2nd read following an exposure of ≥80% of full well, while the goal is <0.01% under the same constraints as specified for the requirement.

The IDTL's persistence experiment is constructed such that variations in wavelength, fluence and number of detector resets can be explored. The experiment is performed using J, K and M band-pass filters, with three fluence levels (30%, 100% and 1000% of full well) for each band and 3 reset modes (1 reset, 3 resets and autoflush) for each filter-fluence combination. The autoflush mode entails a continuous row-by-row reset of the detector, while the other modes proscribe a specific number of row-by-row resets to be performed between the illumination of the detector and the acquisition of a persistence data cube.

The experiment strategy involves exposing the detector array to various fluence levels and measuring the amount of persistent charge liberated in subsequent science exposures as a function of wavelength. Currently, these science exposures are taken in "sampled up-the-ramp" (SUTR) mode, wherein a series of nondestructive reads are obtained at equally spaced time intervals throughout the total selected exposure time. Exposures consisting of 32 reads in a 2000-second exposure time are typically used when performing this experiment in the IDTL.

The data acquisition process begins with a series of dark exposures, taken with both of the IDTL dewar's filter wheels commanded to the cold blank positions. These dark exposures are taken with the same read mode and exposure time that will later be used for the persistence exposures. In practice, the experiment is started at a point in time at which the detector has not been exposed to light for several hours, in order to minimize the effects of persistence from previous illumination on these dark exposures

The illumination source is then activated, and the filter wheels are commanded to place the first desired filter combination (band-pass filter + one or more neutral density filters) in the beam. A shortest-possible CDS (Fowler-1) is then taken. The signal level in this exposure is used to estimate the flux (in ADU/sec/pixel) produced by the illumination source through the filter combination. The flux and the detector full well value (supplied as an input parameter) are used to calculate the illumination exposure times required to produce the desired fluence levels at the detector array. This process is repeated with the remaining desired filter combinations.

The operations outlined in the previous paragraph involve exposing the array to illumination, and this may result in the retention of some persistent charge. Therefore, both filter wheels are closed and a waiting period (currently about 3 hours) is enforced in order to allow this charge to be liberated prior to resuming the experiment.

Next, the illumination source is activated and the filter wheels are commanded to place the first desired filter combination back into the light path. The detector is exposed to light for the amount of time calculated to produce the lowest desired fluence level. A SUTR image is obtained during the time of illumination; this involves a single row-by-reset of the detector array prior to the readout of the image. The illumination image is then written to disk in FITS format, the filter wheels are rotated to the cold blank positions, and a persistence exposure is obtained. There is a single row-by-row reset of the array at the beginning of the persistence exposure, and additional resets can be performed in the time between the end of the detector's illumination and the start of the persistence exposure if desired. The fluence time (total time the detector was exposed to light) and the delay time (the time between the end of detector illumination and the beginning of the persistence exposure) are recorded in the FITS header of the persistence image. These steps are

repeated to produce persistence exposures for the remaining fluence levels. After all fluence levels have been generated for the first filter combination, the process is repeated for the rest of the chosen filter combinations.

After all of the data have been acquired, the reduction process begins with operations on the dark exposures. For each dark exposure, the first read is subtracted from all subsequent reads to correct for bias effects. We subtract reference pixel data from the active pixel data (except for data in the first read) in order to remove drifts. A new dark image cube is created out of the median of each pixel's value in all of the dark exposures in order to remove cosmic ray contamination. The first two steps are repeated on the persistence images. We remove dark current from the persistence images by subtracting the dark image cube.

These dark-subtracted persistence images have values that represent the amount of persistent charge liberated (in ADU/pixel) as of the time of that read. We convert these values into liberated charge per time interval (between reads) by subtracting values in neighboring reads. Finally, we take the mode of all such values for each interval and plot them. Total cumulative persistence at the time of each read is also plotted along with the differential persistence just described.

The persistent charge amounts (in ADU/pixel) thus obtained are divided by the appropriate fluence level in order to express the results in terms of a percentage of the fluence generated prior to beginning the persistence exposure.

A summary of results is shown in the tables below. Note that the persistence values shown in the table represent cumulative persistence in 2000 seconds, not the value in the 2^{nd} read after a saturating exposure. That value can be read from persistence plots like those shown in the figures below.

Figure 27. Cumulative Persistence in 2000 seconds for H2RG-015-5.0mu with 1 reset.

1 Reset					
Device	Filter-Fluence	Fluence Time (s)	Fluence (ADU)	Persistence (%)	Persistence (ADU)
H2RG-015-5.0mu	J-30%	60.9	23000	0.28	64
	J-100%	245.8	94000	0.19	179
	J-1000%	2583.3	986000	0.04	355
	K-30%	63.0	25000	0.24	60
	K-100%	238.6	96000	0.18	173
	K-1000%	2477.2	996000	0.04	359
	M-30%	68.2	26000	0.21	55
	M-100%	254.1	96000	0.19	182
	M-1000%	2589.5	979000	0.04	352

Figure 28. Cumulative Persistence in 2000 seconds for H2RG-015-5.0mu with 3 resets.

1 Reset					
Device	Filter-Fluence	Fluence Time (s)	Fluence (ADU)	Persistence (%)	Persistence (ADU)
SB304-008-5.0mu	J-30%	57.5	16000	2.90	464
	J-100%	222.8	62000	3.20	1984
	J-1000%	2334.9	647000	0.38	2459
	K-30%	63.1	18000	2.60	468
	K-100%	228.0	64000	3.20	2048
	K-1000%	2326.4	649000	0.38	2466
	M-30%	47.1	17000	3.40	578
	M-100%	178.2	63000	3.20	2016
	M-1000%	1832.4	648000	0.39	2527

Figure 29. Cumulative Persistence in 2000 seconds for H2RG-015-5.0mu with 3 resets.

3 Resets					
Device	Filter-Fluence	Fluence Time (s)	Fluence (ADU)	Persistence (%)	Persistence (ADU)
H2RG-015-5.0mu	J-30%	60.4	23000	0.10	23
	J-100%	244.3	94000	0.06	58
	J-1000%	2583.1	990000	0.02	198
	K-30%	63.0	25000	0.08	21
	K-100%	238.2	96000	0.06	61
	K-1000%	2473.8	996000	0.02	209
	M-30%	67.1	26000	N/A	N/A
	M-100%	251.2	96000	0.06	58
	M-1000%	2589.8	990000	0.02	208

Figure 30. Cumulative Persistence in 2000 seconds for SB304-008-5.0mu with 3 resets.

3 Resets					
Device	Filter-Fluence	Fluence Time (s)	Fluence (ADU)	Persistence (%)	Persistence (ADU)
SB304-008-5.0mu	J-30%	57.4	16000	0.82	131
	J-100%	222.2	62000	1.60	992
	J-1000%	2326.0	647000	0.22	1423
	K-30%	63.3	18000	0.82	148
	K-100%	226.6	63000	1.80	1134
	K-1000%	2316.5	649000	0.23	1493
	M-30%	N/A	N/A	N/A	N/A
	M-100%	176.9	63000	1.60	1008
	M-1000%	1817.9	648000	0.23	1490

Figure 31. Cumulative Persistence in 2000 seconds for H2RG-015-5.0mu with autoflush.

Autoflush					
Device	Filter-Fluence	Fluence Time (s)	Fluence (ADU)	Persistence (%)	Persistence (ADU)
H2RG-015-5.0mu	J-30%	74.1	34000	0.04	14
	J-100%	226.8	105000	0.03	32
	J-1000%	2174.4	1005000	0.02	151
	K-30%	92.7	37000	0.03	13
	K-100%	269.5	107000	0.03	35
	K-1000%	2417.3	956000	0.02	153
	M-30%	93.7	36000	N/A	N/A
	M-100%	274.5	106000	0.03	30
	M-1000%	2416.6	932000	0.02	149

Figure 32. Cumulative Persistence in 2000 seconds for SB304-008-5.0mu with autoflush.

Autoflush					
Device	Filter-Fluence	Fluence Time (s)	Fluence (ADU)	Persistence (%)	Persistence (ADU)
SB304-008-5.0mu	J-30%	N/A	N/A	N/A	N/A
	J-100%	227.8	65000	1.06	689
	J-1000%	2280.4	650000	0.16	1040
	K-30%	N/A	N/A	N/A	N/A
	K-100%	239.4	67000	1.05	704
	K-1000%	2338.8	652000	0.16	1043
	M-30%	N/A	N/A	N/A	N/A
	M-100%	192.2	67000	0.87	583
	M-1000%	1863.3	653000	0.16	1045

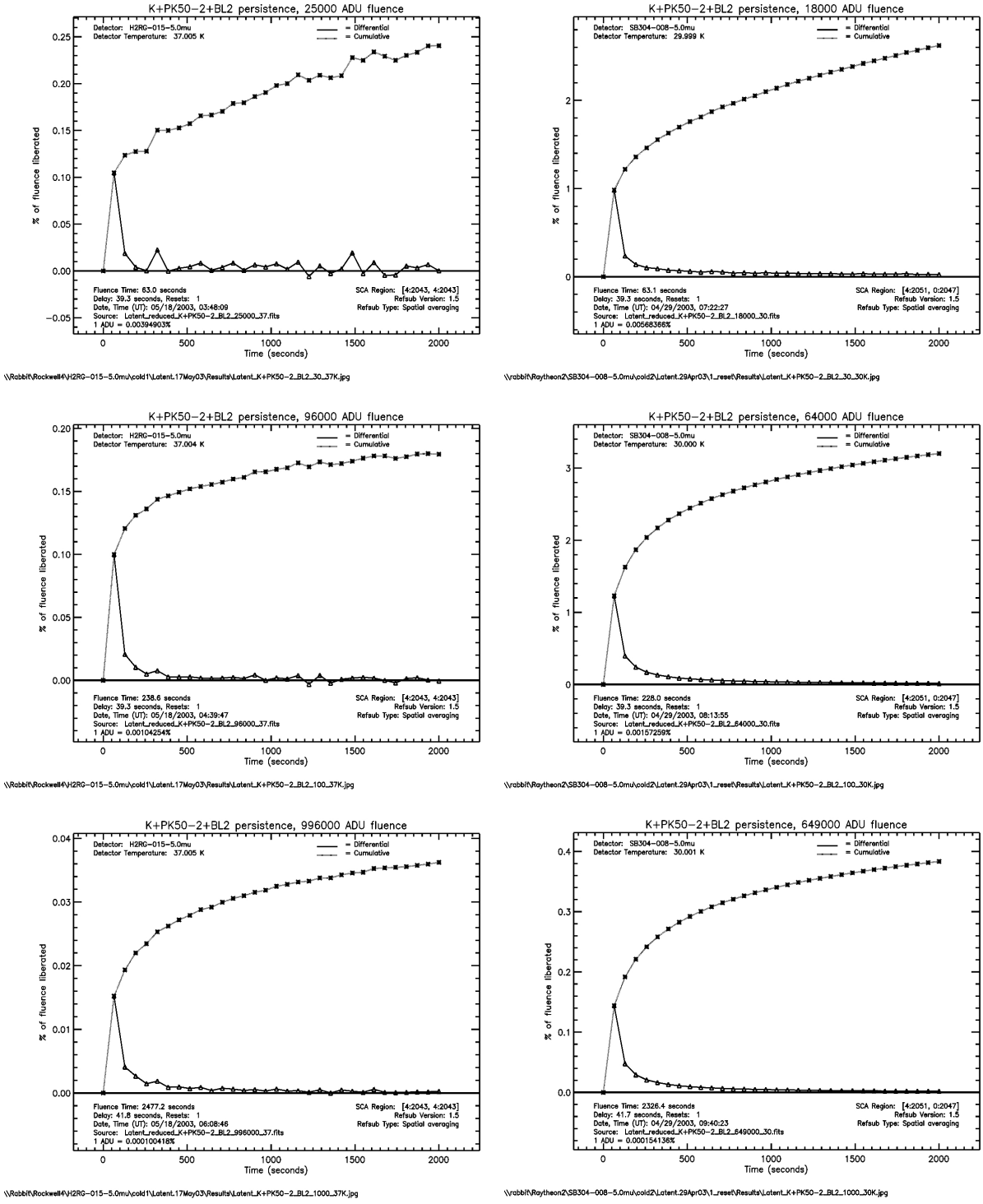

Figure 33: One-reset persistence for Rockwell H2RG-015-5.0mu (top row) and Raytheon SB304-008-5.0mu (bottom row). Results are for the K+PK50-2+BL2 filter combination. The notation "BL2" refers to a combination of two 1% Inconel neutral density filters, while "PK50-2" refers to a 2-mm thick PK50 filter.

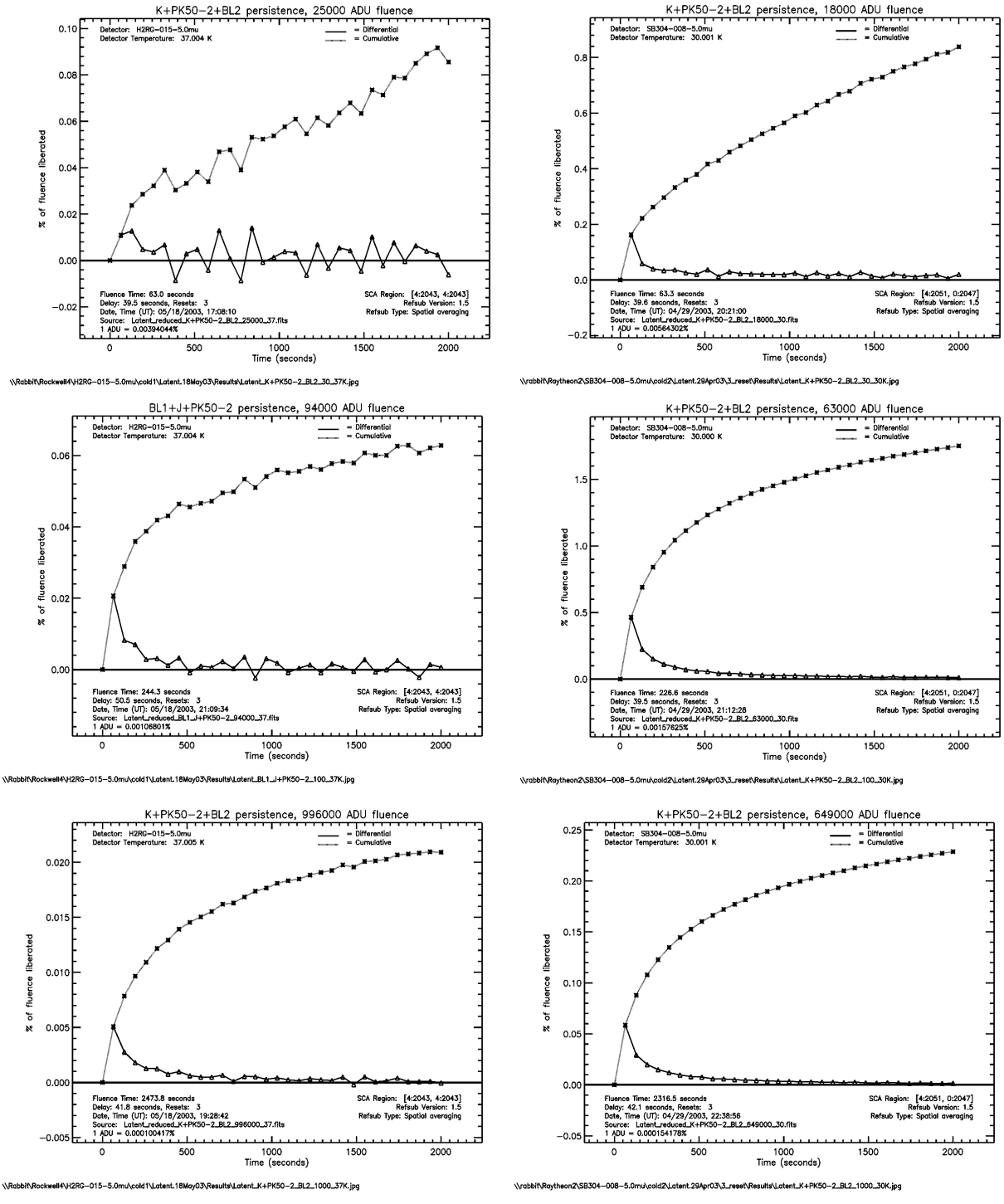

Figure 34: Three-reset persistence for Rockwell H2RG-015-5.0mu (top row) and Raytheon SB304-008-5.0mu (bottom row). Results are for the K+PK50-2+BL2 filter combination. The notation "BL2" refers to a combination of two 1% Inconel neutral density filters, while "PK50-2" refers to a 2-mm thick PK50 filter.

9. CROSSTALK

The IDTL crosstalk experiment measures a combination of three different effects. The first of these is electronic crosstalk, or the effect induced in an analog channel by a signal in a neighboring channel. The second effect is charge diffusion, where charge liberated in a pixel hit by a cosmic ray migrates to neighboring pixels. The third effect is incomplete settling, where the time between pixel resets is insufficient to allow signal settling before the beginning of the read of the next pixel. The word "crosstalk" when not specified as "electronic crosstalk" refers to the combination of these three effects in this document.

The crosstalk experiment makes use of the data collected for the dark current/read noise experiment (250 reads, sampled continuously up-the-ramp for 2700 seconds). The goal of the experiment is to detect cosmic ray hits in the input ramps and characterize crosstalk by measuring signal in pixels adjacent to hit pixels relative to the signal in the hit pixel. The method of characterizing crosstalk used by the IDTL is a modified version of a process developed by Don Hall of the University of Hawaii Institute for Astronomy.

Detector temperature is the only variation considered for this experiment, so the reduction and analysis process begins with the grouping together of input images according to the value of this parameter. For a given detector temperature, the process then continues with the creation of an initial cosmic ray mask for each exposure at that temperature. This mask indicates the locations of pixels that are hit by cosmic rays during the course of the image's exposure time.

The initial cosmic ray mask is constructed for an image by creating 249 difference frames formed by subtracting each read from the next. The median and standard deviation of each of these frames are calculated, and the cosmic ray mask is populated with all pixels that exhibit a value 10 sigmas above the median in one difference frame and do not have a value greater than 3 sigmas above the median in any other difference frame. The masked pixels are thus the ones that experience a huge increase in signal from one read to the next, but are not otherwise unusual. The mask should therefore exclude pixels that are hit by cosmic rays more than once in an exposure as well as pixels that experience elevated dark current. See Figure 4 for an intensity profile of a typical cosmic ray hit.

The initial mask is now refined by rejecting from it all pixels within 5 pixels of the image edge, as this is the region which can be occupied by reference pixels. Cosmic ray hits that do not have higher signal than all of their adjacent pixels are also rejected.

The next step is to construct a processed Fowler-16 frame for each input 250-read ramp. This is accomplished by subtracting the average of the first 16 reads of the ramp from the average of the last 16 reads. The crosstalk results are computed from these frames, and they are also used to further refine the initial cosmic ray masks.

The crosstalk reduction procedure now continues on pairs of processed Fowler-16 frames. For a given pair of these frames, denoted by the identifiers p1 and p2, the difference frame d = p1 – p2 is constructed. Taking the difference of the two frames corrects for any residual bias effects, and cosmic ray hits in p1 will now show up as large positive signal values in the frame d. A secondary cosmic ray mask for p1 is now constructed by marking all pixels with signals above a specified threshold. This secondary mask excludes pixels with extremely high dark current that rise to saturation very rapidly—these pixels are sometimes included in the initial mask. Pixels that are members of both the initial and secondary masks are now retained as the final cosmic ray mask for p1.

Now the signal intensity in the masked pixels and their 8 adjacent pixels are recorded from the difference frame d. At this point, a final uniformity criterion is invoked. A cosmic ray hit is rejected if the signal in its four nearest-neighbor pixels varies by more than a factor of six. This is to constrain the cosmic ray hits to those that strike near the center of a pixel and should thus display nearly uniform charge diffusion to directly (non-diagonally) adjacent pixels.

The process outlined in the previous two paragraphs now continues for all of the pairs of processed Fowler-16 frames for a given detector temperature. The result is a collection of 3 x 3 arrays representing the intensity of cosmic ray hits and their adjacent pixels. Each of these arrays is divided by the intensity of the central pixel and multiplied by 100% in order to calculate the crosstalk in adjacent pixels as a percentage of the intensity of the central cosmic ray hit. A

representative 3 x 3 array is then produced by sorting the collection of values at each adjacent pixel position and reporting the value at the 25th percentile as the crosstalk value for that position. The 25th percentile value is chosen in order to reject values that are dominated by the read noise of the detector.

The NIRCam requirement species an upper limit of 5% electronic crosstalk. As previously stated, the IDTL experiment measures a combination of electronic crosstalk with two other effects. The Raytheon SB304 is designed so that a single output reads out every 4th column of the array. Therefore, the IDTL experiment measures charge diffusion and electronic crosstalk for this device, but not incomplete settling. This is due to the fact that the next pixel read after a pixel hit by a cosmic ray is not adjacent to that pixel. Conversely, the Rockwell H2RG is designed so that each output reads out a contiguous quadrant of the array. As a result, the IDTL experiment measures charge diffusion and incomplete settling, but not electronic crosstalk. This is due to the fact that pixels adjacent to a pixel hit by a cosmic ray are all read out by the same output. Since electronic crosstalk is not isolated by the IDTL experiment, it is difficult to measure the results against the NIRCam requirement. The experiment results are shown in the Figures below.

H2RG-015-5.0mu	Detector Temp. (K): 37.0 Number of images: 6 Number of Events: 1295 Crosstalk Results (%):		
	0.15	1.52	0.13
	1.61	100.00	1.63
	0.15	1.50	0.15

SB304-008-5.0mu	Detector Temp. (K): 30.0 Number of images: 2 Number of Events: 304 Crosstalk Results (%):		
	0.00	0.53	0.01
	0.77	100.00	0.75
	0.00	0.50	0.02

Figure 35: Crosstalk results shown at the optimum operating temperature for the Rockwell (left) and Raytheon (right) devices

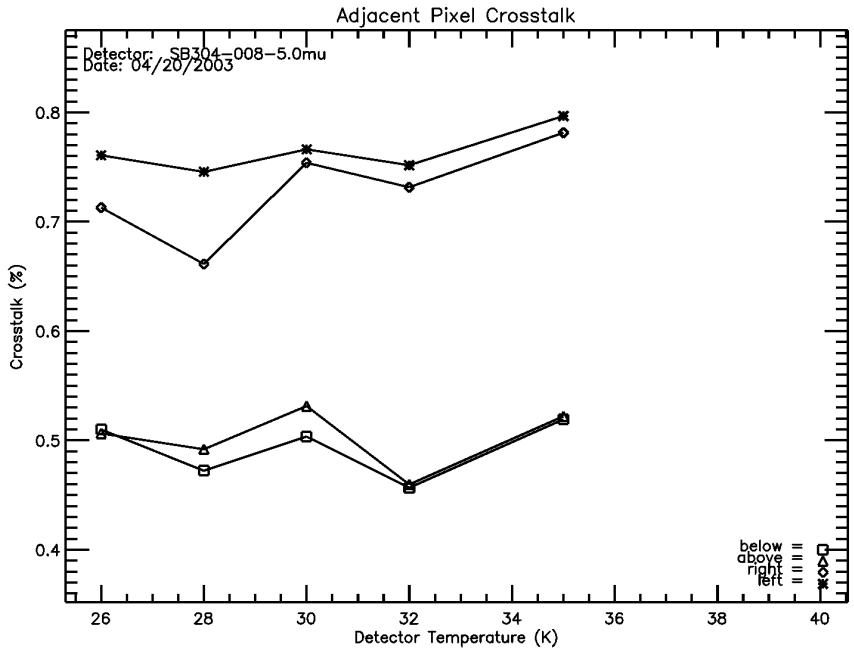

Figure 36: Crosstalk vs. detector temperature for Raytheon SB304-008-5.0mu.

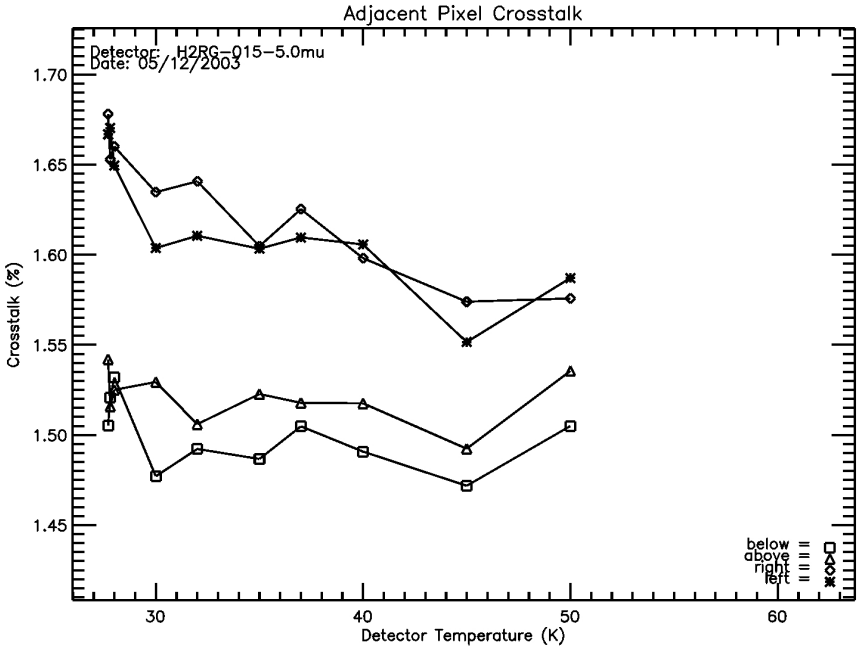

Figure 37: Crosstalk vs. detector temperature for Rockwell H2RG-015-5.0mu.

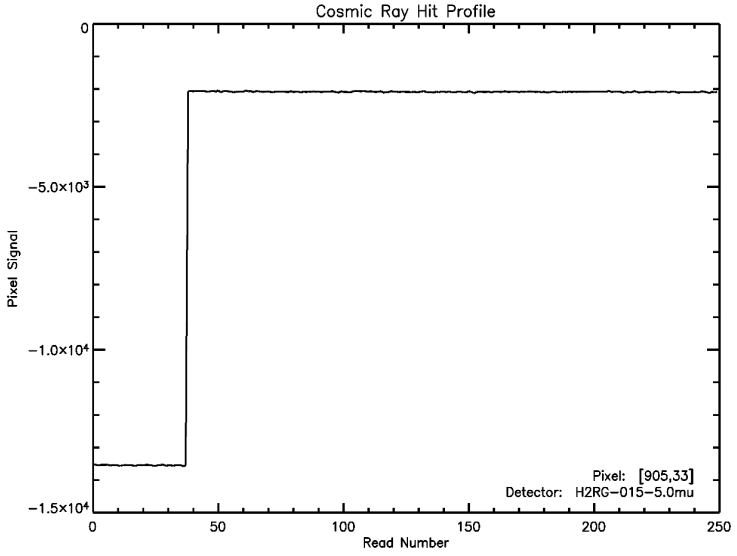

Figure 38: Profile of cosmic ray hit in 250-read ramp for Rockwell H2RG-015-5.0mu.

10. DETECTIVE QUANTUM EFFICIENCY (DQE)

DQE is the realized S/N compared to that of an ideal detector. It is often measured in the background-limited case so that it is most closely related to the photon capture process in the bulk material of the detector, as opposed to being related to read noise effects in the post-capture electronics. DQE can vary with wavelength, temperature, and individual pixel properties, to name a few examples.

Pixel-to-pixel variations in QE (relative QE, RQE) result from differences in the crystal structure of the light sensitive material created when the crystal is grown. Other causes are geometrical and can be traced to the manufacturing process: 1) variations in the effective detector area and collecting volume (depletion region), 2) variations of integration capacity, 3) changes in the thickness of the substrate and/or in the antireflection coating. In principle, RQE can be calibrated and corrected, as long as the detector performance remains stable over time. Several phenomena like cosmic rays, thermal cycling, temperature drifts (also related to variations of the radiative thermal background), may change the relative QE and require frequent calibration. Thus, excellent QE stability under these varying conditions is required.

We used two methods to measure DQE. The first method uses a calibrated source and a transmission model of the optics to determine the incident flux at the detector. One can then compare the measured S/N to the ideal S/N that is limited by the shot noise inherent to the incoming beam. The second method uses a calibrated sensor and stable source. In this method, the incident flux at the detector is measured directly by placing the calibrated sensor at the location of the detector and using the source for illumination. As long as the source can reproducibly output the same amount of light at a later time, then one can infer that the incident flux at the detector will be the same as it was at the calibrated sensor. Once again, one can then compare the predicted and realized S/N.

We used both methods, collecting images over a broad range of wavelengths (0.4 and 6.0 μm) and detector temperatures (30 and 40 K). The data are still being calibrated, and we include some figures to demonstrate the short-wave and long-wave cutoff performance of the detectors. Note that experimental effects can be seen in these figures, such as the monochromator grating function, optical transmission function, and the spectral energy distribution of the source (which is steeply declining towards shorter wavelengths). Despite these effects, one can see that the HgCdTe material has been successfully produced for long-wavelength performance out to somewhat greater than 5.0 μm, and that the substrate removal process on part H2RG-006 was successful in delivering short-wavelength performance.

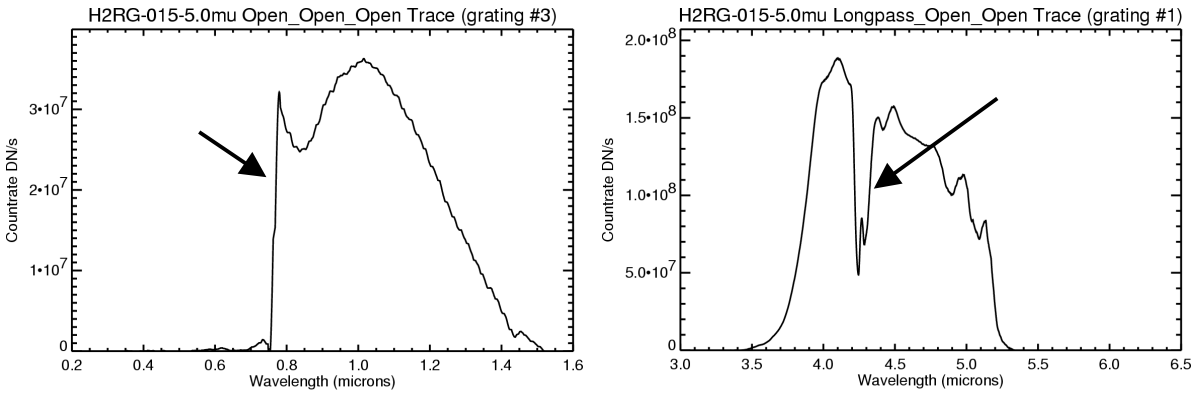

Figure 39. Relative response versus wavelength. The grating function, spectral energy distribution of the source, and optical transfer functions, have not been taken out. Notice the sharp cutoff near 0.8 μm due to the CdZnTe substrate which has not been removed from this particular device. Also, note the excellent performance out to wavelengths longer than 5.0 μm. The CO_2 absorption is atmospheric.

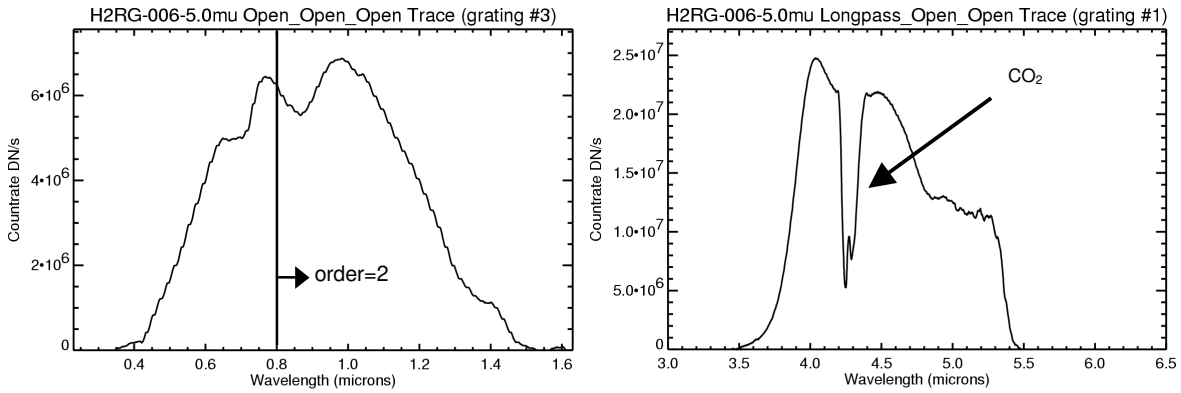

Figure 40. Relative response versus wavelength. The grating function, spectral energy distribution of the source, and optical transfer functions, have not been taken out. Notice the performance below 0.8 μm. The CdZnTe substrate has been removed from this particular device.

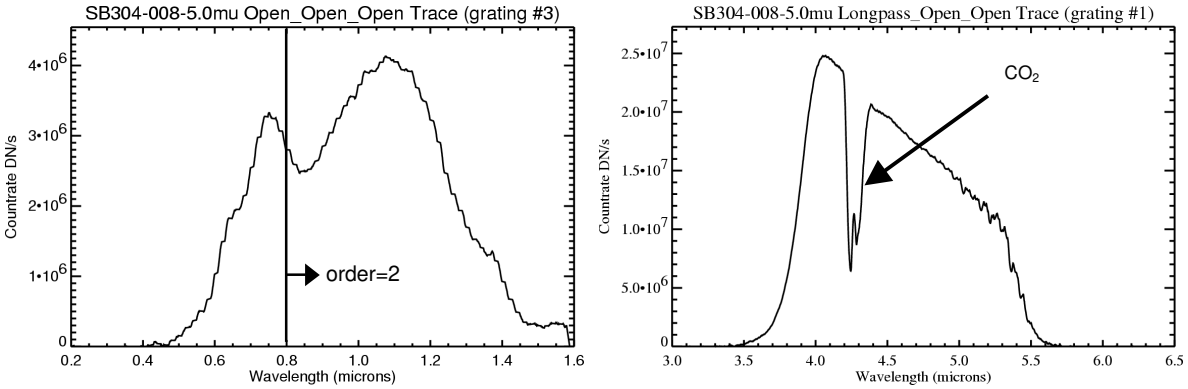

Figure 41. Relative response versus wavelength. The grating function, spectral energy distribution of the source, and optical transfer functions, have not been taken out. The CO_2 absorption is atmospheric.

11. SUMMARY COMPARISONS

The following table lists NIRCam requirements and goals in a variety of detector parameters, along with IDTL measurements, where available. Both detector types show excellent performance, and satisfy many of the requirements, and some of the goals

Table 7. University of Arizona NIRCam requirements and measured detector performance.

Parameter	Requirement	Goal	Raytheon	Rockwell
SCA Format	Minimum of 2048x2048 pixels, with reference pixels located within or outside of the		2048 X2048	2048 X2048
SCA Imaging Surface Flatness	≤ 15 mm peak-to-valley		NA	NA
Pixel Pitch	18 – 25 µm		25	18
Pixel-to-Pixel relative location knowledge	<1/20th *pixel*		NA	NA
Fill Factor	≥ 95%	100%	NA	NA
Bad Columns/Rows	<5 columns/rows containing >1000 contiguous out of spec		NA	NA
Bad Pixel Clustering	<20 clusters containing up to 20 contiguous out of spec pixels.		NA	NA
Pixel Operability (while simultaneously meeting all requirements)	> 98%		NA	NA
Total Noise (Quadrature sum of all sources) per pixel in 1000 s*	≤ 9 e^- rms	≤ 2.5 e^- rms	< 13 e-	< 10 e-
Read noise for a single read	≤ 15 e^- rms	≤ 7 e^- rms	10 e^-*	12 e^-*
Dark current	< 0.01 e/sec		0.006 e^-/s	0.001 e^-/s
Minimum Detective Quantum Efficiency	≥70% for 0.6 < l < 1.0 µm; ≥80% for 1.0 ≤ l < 5.0 µm.	≥90% for 0.6 < l < 1.0 µm;		
Well Capacity	6×10^4 e^-	2×10^5 e^-	10% non-lin: 0.77(10^5) e^- saturation: 1.22(10^5) e^-	10% non-lin: 1.04(10^5) e^- saturation: 1.30(10^5) e^-
Electrical crosstalk between adjacent pixels	≤ 5%	≤ 2%	0.75%	1.64%
Radiometric Stability	1% over 1000s	< 1% over 1000s	NA	NA
Latent or Residual Images, when measured at the same integration time as was used for the near saturation image.	<0.1% after the 2nd read following an exposure of ≥80% of full well	<0.01% after the 2nd read following an exposure of ≥80% of full well	0.90%	0.02%
Radiation Immunity after exposure to 6Krad TID (Si)	<4% pixels out of spec at 6kRad TID Si	<0.5% pixels out of spec at 6kRad TID Si	NA	NA
Cosmic Ray Pixel Upsets in 1000s and cosmic ray flux of 5 s^{-1} cm^{-2}.	<10% pixels above noise requirement	<2% pixels above noise requirement	NA	NA
Frame Read-out Time	12 s	<12 s	10.7 s	10.7 s
SCA pixel readout rate	100kHz rate, 10ms/ pixel.	>100kHz rate	100 kHz	100 kHz
Sub-array Size	As large as 128 x 128 pixels		NA	NA
Sub-array exposure time	0.2 sec for 128 pixels x 128 pixels, shorter for fewer pixels	< 0.2 secs for 128 pixels x 128 pixels	NA	NA

*Estimated using digitally filtered data.

12. ACKNOWLEDGEMENTS

We thank the following individuals for a very productive collaboration: Al Fowler (NOAO), Gert Finger (ESO), James Garnett and Kardri Vural (Rockwell), Ken Ando, Peter Love, and Alan Hoffman (Raytheon), Craig McCreight (NASA/ARC), Matt Greenhouse (NASA/GSFC), Judy Pipher, Bill Forrest, Craig McMurtry, and Drew Moore (U. Rochester), and Don Hall (U. Hawaii). This work was supported, in part, by NASA, under awards No. NAG5-10430 and NAG5-13317.

13. REFERENCES

Figer, D. F., Agronin, M., Balleza, J., Barkhouser, R., Bergeron, L., Greene, G. R., McCandliss, S. R., Rauscher, B. J., Reeves, T., Regan, M. W., Sharma, U., Stockman, H. S. 2003, SPIE, 4850, 981

Rauscher, B. J., Figer, D. F., Agronin, M., Balleza, J., Barkhouser, R., Bergeron, L., Greene, G. R., McCandliss, S. R., Reeves, T., Regan, M. W., Sharma, U., Stockman, H. S. 2003, SPIE, 4850, 962